Physically based statistical integration of TRMM microwave measurements for precipitation profiling

Sabatino Di Michele,[1] Frank S. Marzano,[2] Alberto Mugnai,[1] Alessandra Tassa,[1] and José Pedro V. Poiares Baptista[3]

Received 4 March 2002; revised 1 August 2002; accepted 11 September 2002; published 19 June 2003.

[1] A statistical methodology to combine measurements from space-borne microwave radar and radiometers is proposed. The approach is fairly general, even though the combination technique is here tailored for the two instruments onboard the Tropical Rainfall Measuring Mission (TRMM) satellite specifically devoted to rainfall measurements, that is, the Precipitation Radar (PR) and the TRMM Microwave Imager (TMI). Two combined retrieval algorithms are proposed, both derived from the previously developed Bayesian algorithm for microwave-based precipitation retrieval from passive sensors (BAMPR-P), which is based on a Bayesian inversion method and is trained by a modeled cloud radiation database. The first combined technique, called BAMPR-C (BAMPR combined), operates in the narrower common swath aiming at exploiting the simultaneous measurements of PR and TMI instruments. Within BAMPR-C the hydrometeor profiles, retrieved from TMI, are used as a constraint for the PR-based inversion: this two step cascade allows us to overcome the difficulty to take into account the different scan geometries of TMI and PR. The second combined technique is called BAMPR-B (BAMPR broadening) and aims at improving the TMI-only retrieval outside the common swath. In this approach, first optimal retrieved profiles are generated by reversing the order of the previous two steps of BAMPR-C cascade within the common swath. Then the resulting profile data set and the corresponding TMI brightness temperatures are used to define the cloud radiation database to be employed outside the common swath for the TMI-only retrieval, achieving the so-called radar swath synthetic broadening. Numerical internal tests, using simulated data, are illustrated to quantify the features of the proposed synergetic algorithms. Finally, an application to measured TRMM data for a selected case study (hurricane Bonnie on August 1998) is shown and discussed. *INDEX TERMS:* 3354 Meteorology and Atmospheric Dynamics: Precipitation (1854); 3360 Meteorology and Atmospheric Dynamics: Remote sensing; 3394 Meteorology and Atmospheric Dynamics: Instruments and techniques; *KEYWORDS:* rainfall, microwave radiometer, precipitation radar, TRMM

Citation: Di Michele, S., F. S. Marzano, A. Mugnai, A. Tassa, and J. P. V. Poiares Baptista, Physically based statistical integration of TRMM microwave measurements for precipitation profiling, *Radio Sci., 38*(4), 8072, doi:10.1029/2002RS002636, 2003.

1. Introduction

[2] The presence aboard the Tropical Rainfall Measuring Mission (TRMM) platform of the first space-borne Precipitation Radar (PR) has represented a new incentive for developing new precipitation retrieval techniques based on satellite microwave measurements. The coexistence of PR with the TRMM microwave imager (TMI) has been soon identified as a unique feature to be exploited in the long-standing process of improving rain retrieval accuracy from space.

[3] In the last decade the use of a physical approach, based on cloud radiative model simulations, has reached a mature stage for the precipitation profile retrieval, especially from passive microwave measurements [*Mugnai et al.*, 1993; *Kummerow et al.*, 1996; *Pierdicca et al.*, 1996]. Three-dimensional (3-D) cloud-model simulations, used as inputs to microwave radiative transfer algorithms, have been adapted to generate large data-

[1] Istituto di Scienze dell'Atmosfera e del Clima (ISAC), Consiglio Nazionale delle Ricerche (CNR) Rome, Italy.

[2] Dipartimento di Ingegneria Elettrica, Centro di Eccellenza CETEMPS, Università dell'Aquila, Monteluco di Roio, L'Aquila, Italy.

[3] European Space Research and Technology Centre, European Space Agency, Noordwijk, Netherlands.

Copyright 2003 by the American Geophysical Union.
0048-6604/03/2002RS002636$11.00

bases consisting of cloud/precipitation profiles and associated upwelling brightness temperatures (TBs) at given frequencies and viewing angles. Within most physical inversion procedures, the precipitating cloud profile retrieval is based on the statistical matching between observed and simulated TBs by means of proper error weights and a priori information.

[4] The extension of this approach to incorporate radar measured reflectivities, as predictors additional to TBs, has been proposed using airborne measurements [*Olson et al.*, 1996; *Haddad et al.*, 1996; *Marzano et al.*, 1999; *Marzano and Bauer*, 2001; *Grecu and Anagnostou*, 2002]. When dealing with radar and radiometer combination, a major issue is represented by their respective scan geometry. For airborne applications, both sensors generally scan across track so that their measurements can be easily matched. For spaceborne platforms, and specifically for TRMM, radar and radiometer can exhibit different scanning configuration which prevent from a direct implementation of retrieval techniques developed for airborne sensors [*Haddad et al.*, 1997; *Marzano et al.*, 1999]. Another important issue is to distinguish observed areas, where radar and radiometer measurements are both available ("inside the common swath"), from those where radar and radiometer data are available only in a sub-domain and in the entire domain, respectively ("outside the common swath"). A typical example of the latter case is represented by TRMM where PR swath overlaps only the central portion of TMI one [*Kummerow et al.*, 1998].

[5] In this work, two synergetic physically based retrieval techniques for integrating spaceborne microwave radar and radiometer measurements are proposed to address the above mentioned issues. Both techniques evolve from the Bayesian algorithm for microwave-based precipitation retrieval from passive sensors (BAMPR-P), which is based on a Bayesian inversion method trained by a modeled cloud radiation database [*Marzano et al*., 2000; *Mugnai et al*., 2001; *Tassa et al.*, 2003]. The basic principle of sensor synergy, here illustrated, is founded on the consideration that a rain radar mainly senses the liquid hydrometeor profile, while a microwave radiometer is sensitive to ice amount at higher frequencies and to integrated liquid water at lower frequencies. The developed statistical methodology is of general use, even though here it specifically focused on PR and TMI data. Nevertheless, since the core satellite of the proposed Global Precipitation Mission (GPM) has a radar and a radiometer having the same basic configuration, a straightforward extension of the proposed methodology to GPM can be envisaged [*Mugnai et al.*, 2002].

[6] Both the proposed algorithms are explicitly designed also to overcome this difficulty in matching the instruments. The first combined retrieval technique is able to provide estimated vertical content of hydrometeor profiles and surface rain rate at the horizontal resolution of the PR, exploiting the radiometric information of the upper portions of the profiles within the common PR-TMI swath. The second inversion technique essentially aims at extending the detailed information given by PR measurements to the portion of the swath where only TMI measurements are present.

[7] The paper is organized as follows. First, a general description of the methodology is given in sections 2 and 3 both for the forward and the inverse problem. Then, results of numerical tests on synthetic measurements are shown in section 4. Finally, in section 5 an application to TRMM data is illustrated.

2. Cloud-Resolving Radiative Modeling

[8] In this section the procedure for generating the cloud radiation database for combined radar and radiometric observations will be summarized. Additional details are given by *Tassa et al.* [2003], where issues related to radiative transfer modeling are discussed.

2.1. Cloud-Resolving Model

[9] The starting point of the cloud radiation database (CRD) generation is the 3-D output of a cloud model simulation. In this study we have made use of the simulation of a tropical cyclone (hurricane Bonnie, occurred in August 1998), performed by the University of Wisconsin Non-hydrostatic Modeling System (UW-NMS) [*Tripoli*, 1992]. This simulation is characterized by a horizontal domain of 200 by 200 grid points with 2.5-km horizontal resolution. The vertical structures are specified over 35 levels from 0 to 20 km height. Details on this simulation are given by *Panegrossi et al.* [2001] and *Tassa et al.* [2003].

[10] The cloud microphysics includes a parameterized two-type liquid phase scheme (cloud and rain) and a parameterized four-type categories ice phase (*i.e*., pristine ice, snow, graupel and aggregates). In the model water cloud and pristine ice particles are monodispersed, while inverse-exponential size distributions are assumed for the other hydrometeors. Graupel density is constant (0.6 g/cm^3), while snow and aggregates have size-dependent densities as by *Panegrossi et al.* [1998].

[11] As an example, Figure 1 shows a vertical cross section of rain and graupel equivalent liquid water contents (LWCs) derived from the UW-NMS outputs of Bonnie hurricane simulation at minute 2130 from the initial time step. Effects of rainbands and the presence of convective regions, characterized by higher graupel contents aloft, can be observed.

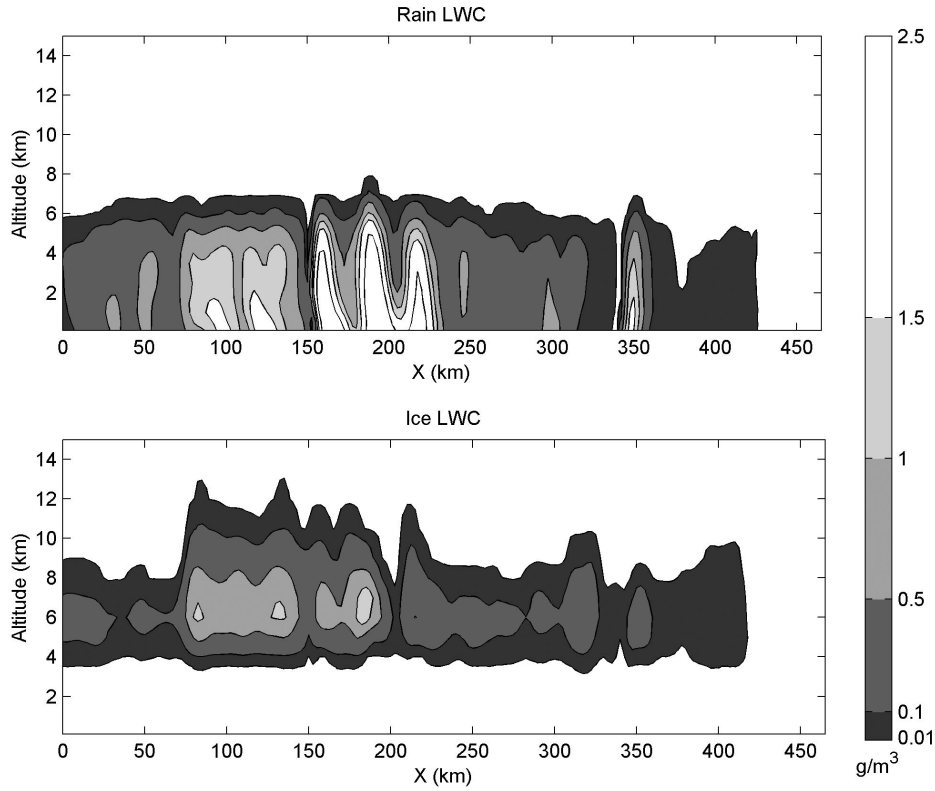

Figure 1. Hurricane Bonnie simulation, minute 2130: vertical cross sections of (top) rain and (bottom) graupel equivalent LWC.

2.2. Simulation of Spaceborne Radiometric and Radar Observations

[12] Upwelling TBs at the top of the atmosphere are computed by means of a simplified 3-D radiative transfer model at TMI viewing angle [*Roberti et al*., 1994; *Bauer et al*., 1998]. For computing the TBs a wind-driven emissivity model is used for sea surface background. Inverse-exponential particle distributions have been used, consistently with the cloud model. The upwelling TBs have been computed at model resolution and successively averaged to mach TMI resolution at the various frequencies.

[13] Figure 2 shows the simulated TMI brightness temperatures at 10, 19, 37 and 85 GHz relative to the cross section in Figure 1, together with the rain and ice columnar contents (along the TMI viewing direction and at the resolution of the 37 GHz channels). As expected, TBs at lower frequencies are sensitive to rain content, while higher-frequency TBs significantly decrease in correspondence of the largest ice contents. Details about the different response of the TMI channels to the various cloud microphysics are given by *Mugnai et al.* [1993].

[14] For simulating the response of a spaceborne radar, the equivalent reflectivity factor Z_{ei} (hereinafter, simply reflectivity) is assumed to be constant within the *i*th layer and given by:

$$Z_{ei} = \frac{\lambda^4}{\pi^5 |K|^2} \int_0^\infty \sigma_b(r) N(r) dr \qquad (1)$$

where λ is the wavelength, K the refractive-index polarizability ($|K|$ is equal to 0.93 for liquid water at 13.8 GHz), the backscattering cross section, N(r) the particle number density and r the particle radius. The attenuated average equivalent reflectivity factor (in $mm^6\ m^{-3}$) due to the *i*th cloud model layer and observed at the platform altitude, has been computed as follows [*Marzano et al.*, 1999]:

$$Z_i = Z_{ei} \frac{1 - e^{-2\tau_i}}{2\tau_i} e^{-2\tau_{i_0}} \qquad (2)$$

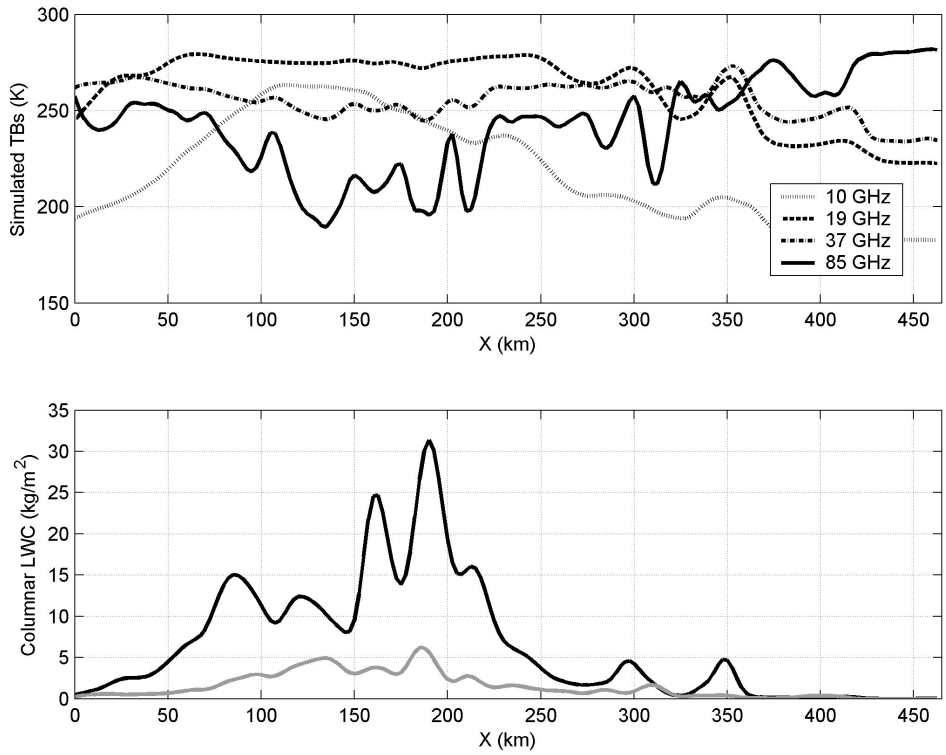

Figure 2. (top) Columnar contents of rain (solid line) and graupel (shaded line) corresponding to the vertical cross section shown in Figure 1. (bottom) Simulated TMI brightness temperatures at 10, 19, 37, and 85 GHz, vertical polarization.

being τ_i the optical thickness of the *i*th layer, τ_{i0} the optical thickness from the top of the *i*th layer to the radar antenna altitude. For each cloud profile, the total path attenuation (*a*, in dB) has been considered as an additional predictor:

$$a = 4.343 \sum_{i=1}^{n} \tau_i \qquad (3)$$

where n is the number of the radar range bins.

[15] In Figure 3 the simulated equivalent reflectivities are shown together with the corresponding attenuated values. By comparing the two, it is important to notice how some of the features that the equivalent reflectivity is able to represent, are ultimately lost in terms of attenuated reflectivity due to the strong path attenuation within the cloud portions characterized by large rain contents.

3. Synergetic Bayesian Algorithms

[16] Almost all rainfall estimation techniques using microwave measurements employ a probabilistic approach due to the statistical nature of precipitating cloud parameters. Our TMI-PR combined retrieval algorithm is based on a Bayesian methodology. In this section, we will first sketch the theoretical foundations of the Bayesian method in the case of only one sensor, then we will describe the extension of the algorithm to combine TMI and PR data.

3.1. Using Single Sensor (TMI)

[17] Using a vectorial notation, we indicate with $\mathbf{g}$ the geophysical (hydrometeor content) vector related to a cloud profile and with $\mathbf{t}_m$ the multispectral vector of TMI measurements (here the subscript "m" will always indicate "measurement").

[18] In the framework of the Bayes estimation theory, a possible optimal estimation is the one which gives the maximum of the a posteriori conditional probability density function (pdf), $p(\mathbf{g}|\mathbf{t}_m)$. This estimate, $\hat{\mathbf{g}}_{MAP}$, is the value of $\mathbf{g}$ such that [*Marzano et al.*, 1999]:

$$\hat{\mathbf{g}}_{MAP} = Mode[\, p(\mathbf{g}|\mathbf{t}_m)] \qquad (4)$$

where *Mode* is the pdf modal value operator. Notice that $\hat{\mathbf{g}}_{MAP}$ is the stationary point corresponding to the abso-

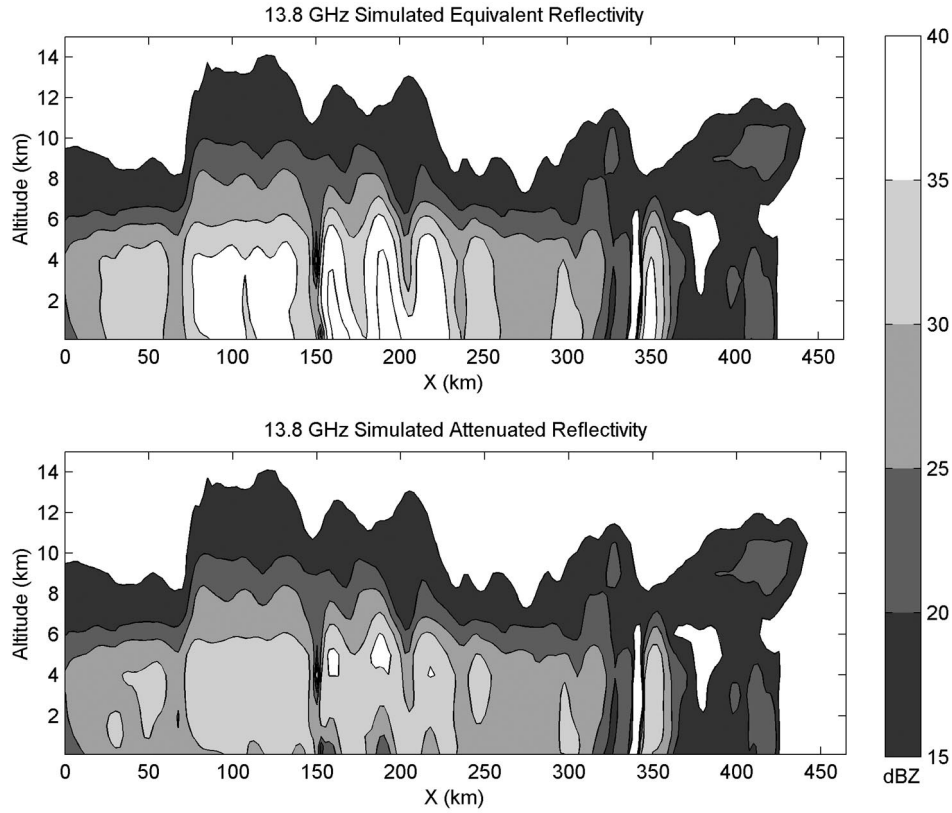

Figure 3. (top) Synthetic PR equivalent reflectivity and (bottom) attenuated reflectivity for the vertical cross section shown in Figure 1.

lute maximum of $p(\mathbf{g}|\mathbf{t}_m)$, being relative maxima erroneous estimates or local traps in the optimization procedure. Equation (4) is referred to as the maximum a posteriori probability (MAP) method.

[19] Another optimal Bayesian criterion is the minimum mean square (MMS), where the estimate $\hat{\mathbf{g}}_{MMS}$ is defined as the expected value of $\mathbf{g}$, given a set of measurements $\mathbf{t}_m$. That is:

$$\hat{\mathbf{g}}_{MMS} = \int_0^\infty \mathbf{g}\, p(\mathbf{g}|\mathbf{t}_m) d\mathbf{g} \tag{5}$$

where the integration is in a multidimensional space with respect to $\mathbf{g}$. Using the Bayes theorem, $p(\mathbf{g}|\mathbf{t}_m)$ can be transformed in the following way to explicitly render the error sources:

$$p(\mathbf{g}|\mathbf{t}_m) = \frac{p(\mathbf{t}_m|\mathbf{g})p(\mathbf{g})}{p(\mathbf{t}_m)} = \frac{p[\varepsilon_t(\mathbf{g})]p(\mathbf{g})}{p(\mathbf{t}_m)} \tag{6}$$

where $p(\mathbf{g})$ is the a priori pdf due to $\mathbf{g}$, and $\boldsymbol{\varepsilon}_t(\mathbf{g}) = [\mathbf{t}_m - \mathbf{t}(\mathbf{g})]$ is the TB error vector with $\mathbf{t}(\mathbf{g})$ the simulated TB vector related to $\mathbf{g}$ by means of the adopted radiative transfer model [*Pierdicca et al.*, 1996; *Marzano et al.*, 1999]. The error vector $\boldsymbol{\varepsilon}_t$ takes into account the radiometric absolute accuracy as well as other possible sources of error due to the forward modeling.

[20] For the BAMPR-P algorithm, a MMS inversion approach is followed, thus making use of equations (5) and (6). For the TB error model $\boldsymbol{\varepsilon}_t(\mathbf{g})$ is assumed a zero-mean random variable Gaussian distribution is assumed. The forward modeling errors have been evaluated through TB sensitivity tests [*Tassa et al.*, 2003]. As for $p(\mathbf{g})$, any attempt to model it with a continuous function can be very often unsuccessful. BAMPR-P approximates the probability density functions $p(\mathbf{g})$ as:

$$p(\mathbf{g}) \sim h(\mathbf{g},\Delta\mathbf{g}) \tag{7}$$

where $h(\mathbf{g},\Delta\mathbf{g})$ is the histogram relative the sample $\mathbf{g}$ within a variable bin $\Delta\mathbf{g}$.

[21] Noting that the cloud radiation database contains a discrete number of profiles (N_{CRD}), the ith

element g(i) of the hydrometeor profile **g** can be estimated approximating equation (5) as follows:

$$\hat{g}_{MMS}(i) = \frac{1}{k}\sum_{j=1}^{N_{CRD}} \hat{g}_j(i) e^{-0.5(\mathbf{t}(\mathbf{g}_j)-\mathbf{t}_m)^T \mathbf{C}_{\varepsilon_t}^{-1}(\mathbf{t}(\mathbf{g}_j)-\mathbf{t}_m)} h(g_j(i),\Delta\mathbf{g}_j) \quad (8)$$

where $\mathbf{g}_j$ is the jth profile sample of the CRD with $g_j(i)$ the ith element, $\mathbf{t}(\mathbf{g}_j)$ the corresponding TB, $\mathbf{C}_{\varepsilon t}$ is the error covariance matrix and k is a normalizing constant:

$$k = \sum_{j=1}^{N_{CRD}} e^{-0.5(\mathbf{t}(\mathbf{g}_j)-\mathbf{t}_m)^T \mathbf{C}_{\varepsilon_t}^{-1}(\mathbf{t}(\mathbf{g}_j)-\mathbf{t}_m)} h(g_j(i),\Delta\mathbf{g}_j) \quad (9)$$

In what follows the description of the combined retrieval algorithms will be done using the more general formulation given by equations (4)-(6), while the numerical implementation can be easily derived using approximations similar to equation (9).

3.2. Using Combined Sensors (TMI and PR)

[22] To combine radar and radiometer measurements, the described Bayesian technique is extended by considering the measured reflectivities in the same way as the radiometric measurements [*Marzano et al.*, 1999]. The simulated multigate radar reflectivities are here indicated by a vector **z** (in $mm^6\ m^{-3}$ or dBZ). Each element of **z** represents the attenuated average reflectivity relative to the ith layer (i.e., to the range gate of the cloud model), as it would be observed by the spaceborne radar. As explained in the previous sub-section, simulated **z** is related to the cloud structure (i.e., to vector **g**) so that it will be referred to as a function **z**(**g**). Synthetic radar measurements $\mathbf{z}_m$ can be obtained by adding a zero-mean Gaussian noise with 1 dBZ variance to the simulated reflectivities **z** when both expressed in $mm^6\ m^{-3}$. Note that in order to make the comparison with PR data possible, the PR reflectivity measurements have been averaged to the vertical resolution of the cloud model with a result still indicated by the vector $\mathbf{z}_m$.

[23] Under the assumption of coincidence between the radiometer and radar beams, radiometric and reflectivity data can be merged to define a new vector of measurements $[\mathbf{t}_m, \mathbf{z}_m, a_m]$. In this case the conditional a posteriori pdf to be considered is $p(\mathbf{g}|\mathbf{t}_m, \mathbf{z}_m, a_m)$, which can be also expressed as follows:

$$p(\mathbf{g}|\mathbf{t}_m, \mathbf{z}_m, a_m) = \frac{p(\mathbf{t}_m|\mathbf{g})p(\mathbf{z}_m|\mathbf{g})p(a_m|\mathbf{g})p(\mathbf{g})}{p(\mathbf{t}_m, \mathbf{z}_m, a_m)} \quad (10)$$

since errors on $\mathbf{t}_m$ $\mathbf{z}_m$, and a_m have been assumed independent to each other.

[24] This extension of the Bayesian approach is sometimes referred to as the "tall-vector" method (TVM) [*Marzano and Bauer*, 2001]. The total path attenuation a_m at 13.8 GHz has been considered as an additional measurement since it has been proved that it can be independently estimated using either PR (surface reference technique, see *Meneghini et al.*, [2000]) or TMI 10 GHz channel [*Smith et al*., 1997]. As discussed by *Olson et al.* [1996] and *Marzano et al*. [1999], the two methods are complementary: the first is more suitable for heavy rain rates, while the second performs better for light-to-moderate ones.

3.2.1. Combined Retrieval Within TRMM: Inside the Common TMI-PR Swath

[25] It has been proved that rain radars exhibit an excellent capability to observe the liquid portion of precipitating clouds. However, considering the reduced sensitivity to ice phase hydrometeors and that the PR minimum detectable signal is around 13 dBZ, the radar-only estimates would suffer of the significant loss of information on the glaciated part of the clouds. In this regard, TMI radiometer can be exploited for a better characterization of the frozen portion of the profile since depressions in the TB measurements at 85 GHz are directly related to the ice content. Thus inside the common swath the addition of TMI TBs to PR reflectivities constitutes a valuable additional information for the knowledge of the upper portion of the observed structure. This basic consideration inspires the whole statistical integration methodology, proposed in this work.

[26] The TVM has been introduced here only as a reference because it is applicable only when the instruments fields of view (FOVs) are collocated, as in the case of airborne measurements. Unfortunately, TMI and PR have different scanning systems: TMI is conically scanning at 53° off-nadir, while PR is cross-track linearly scanning. Moreover, the spatial resolution is also different: each PR bin has a horizontal resolution from 4.4 km at nadir to 7 km at the swath edges, while the TMI FOV ranges from 5 km to 30 km, according to the channel [*Kummerow et al.*, 1998].

[27] Therefore any direct association of TMI TBs with PR reflectivity profiles based on the collocation of the center of the FOVs (either at the ground or at any altitude) results arbitrary since the two instruments do not remotely sense the same scene neither in space nor in time (delay time is about 1 minute for TRMM and will be disregarded here). As consequence, the implementation of TVM to TRMM data is cumbersome. To overcome this difficulty we have found it necessary to separate the combined inversion into two steps in cascade. We will refer to this TMI-PR cascade technique as the BAMPR-C retrieval algorithm (i.e., BAMPR from combined sensors where "C" stands for "combined").

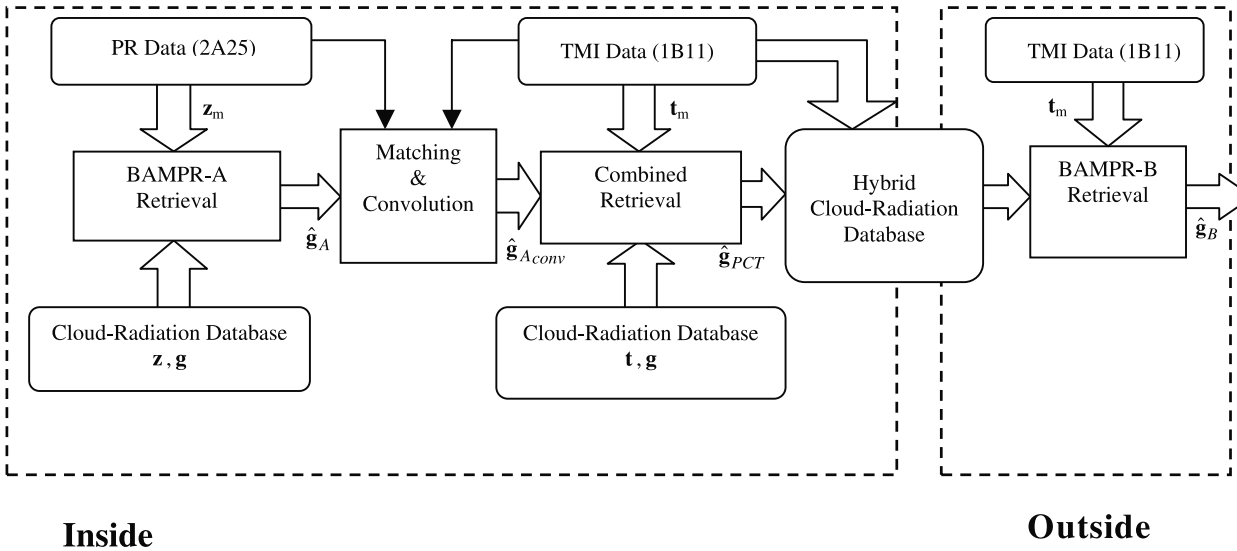

Figure 4. Schematic diagram illustrating the implementation of the Bayesian algorithm for microwave-based precipitation retrieval in the synthetic radar swath broadening configuration (BAMPR-B).

[28] In the first step, a TMI-derived estimation is performed by applying the TMI-only algorithm, that is BAMPR-P. The profiles $\hat{\mathbf{g}}_P$, estimated by BAMPR-P, are slanted and have the resolution of TMI 37 GHz channel. This resolution has been chosen since it has the characteristic of filling completely the TMI swath without overlaps between adjacent FOVs [*Tassa et al.*, 2003]. Contrary to the TVM approach, the matching is now possible because for each altitude range we can associate to each PR reflectivity bin the portion of TMI profiles $\hat{\mathbf{g}}_P$ relative to the same altitude and lying at a minimum distance. This spatial matching procedure is carried out only for the cloud layers above the freezing level (assumed to be at 4.5 km in this work) since the scope of the algorithm is to improve the PR estimates on the ice portion of the precipitating cloud exploiting TMI measurements.

[29] In the second step, the PR-based retrieval is carried out assuming the TMI-derived hydrometeor profile $\hat{\mathbf{g}}_P$ as a 'pseudomeasurement' which, together with reflectivity and attenuation, constitutes the 'pseudotall vector' of measurements $[\hat{\mathbf{g}}_P, \mathbf{z}_m, a_m]$. Then, the conditional a posteriori pdf in this second step of BAMPR-C is $p(\mathbf{g}|\hat{\mathbf{g}}_P, \mathbf{z}_m, a_m)$ which, according to the Bayes theorem, can be expressed as follows:

$$p(\mathbf{g}|\hat{\mathbf{g}}_P, \mathbf{z}_m, a_m) = \frac{p(\hat{\mathbf{g}}_P|\mathbf{g})p(\mathbf{z}_m|\mathbf{g})p(a_m|\mathbf{g})p(\mathbf{g})}{p(\hat{\mathbf{g}}_P, \mathbf{z}_m, a_m)} \quad (11)$$

By comparing equations (10) and (11), it emerges that $\hat{\mathbf{g}}_P$ (which is obtained from $\mathbf{t}_m$) replaces $\mathbf{t}_m$ itself, inserting the radiometer-derived information within the measurement set. As an alternative to maximize equation (11) using a MAP method, we have adopted an MMS estimation approach so that the BAMPR-C estimated profile $\hat{\mathbf{g}}_C$ is obtained from:

$$\hat{\mathbf{g}}_C = \int_0^\infty \mathbf{g}\, p(\mathbf{g}|\hat{\mathbf{g}}_P, \mathbf{z}_m, a_m)d\mathbf{g} \quad (12)$$

where the MMS subscript of $\hat{\mathbf{g}}_C$ has been removed for brevity (see equation (5)).

3.2.2. Combined Retrieval Within TRMM: Radar Swath Synthetic Broadening

[30] As already mentioned, TMI has a much larger swath than PR (i.e., 760 km vs. 220 km). This configuration raises a new intriguing issue in the synergetic retrieval methodology: the feasibility of a synthetic broadening of the PR swath in order to achieve an improvement of TMI estimation accuracy outside the narrow PR swath. In our approach, this can be done adding the physical information derived from PR measurements to select the best portion of the CRD to be used outside the common swath, where only TMI is available. To this purpose we have developed the BAMPR retrieval algorithm for swath broadening (BAMPR-B where "B" stands for "broadening").

[31] For sake of clarity, it is useful to describe the BAMPR-B algorithm distinguishing the stages referring to the common portion of the TMI swath common to PR (inside) from the one where broadening has to be performed (outside). In Figure 4 are represented the different stages composing the two main blocks.

3.2.2.1. Inside the PR/TMI Common Swath

[32] The capitalization of the combined radar-radiometer observations is achieved performing within the common swath a combined cascade in which the two steps, described in section 3.2.1 are reversed. The first step consists of a Bayesian retrieval performed using PR measurements only (referred to as BAMPR-A where "A" stands for "active"). In a strict analogy to (5), BAMPR-A profile estimates $\hat{\mathbf{g}}_A$ are derived from measured PR reflectivity vector $\mathbf{z}_m$ through:

$$\hat{\mathbf{g}}_A = \int_0^\infty \mathbf{g} p(\mathbf{g}|\mathbf{z}_m) d\mathbf{g} \tag{13}$$

where $p(\mathbf{g}|\mathbf{z}_m)$ is the conditional pdf of $\mathbf{g}$ to $\mathbf{z}_m$ [*Marzano et al.*, 1999].

[33] Since the resulting profiles $\hat{\mathbf{g}}_A$ are nearly vertical within the PR swath (due to its scanning between $\pm 17°$) and have an horizontal resolution of 4.5 km, they have to be tilted according to the TMI viewing angle and convolved to the horizontal resolution of TMI estimates at 37 GHz FOV. The previous operations provide a product $\hat{\mathbf{g}}_{A,conv}$ which is compatible with the one obtained by using the BAMPR-P algorithm.

[34] In the second step, the matched PR-based estimation is used as an additional predictor for the TMI-based retrieval. This procedure of the swath broadening technique is here called PR-TMI cascade (PTC) in order to differentiate it from the TMI-PR technique previously introduced to define BAMPR-C. The estimated profiles obtained from PTC are derived again using the MMS approach through:

$$\hat{\mathbf{g}}_{PTC} = \int_0^\infty \mathbf{g}\, p(\mathbf{g}|\mathbf{t}_m, \hat{\mathbf{g}}_{A,conv}) d\mathbf{g} \tag{14}$$

[35] The estimated profiles $\hat{\mathbf{g}}_{PTC}$ can be considered as 'optimal' because they are derived from a microphysically consistent database constrained not only by TB measurements, but also by rain profiles derived from radar estimates. In the above discussion $\hat{\mathbf{g}}_A$ profiles are thought to be retrieved making use of a cloud radiation database, but it is important to point out that the proposed technique holds also in case a different approach is employed for the inversion of the radar measurements.

[36] Each estimated profile $\hat{\mathbf{g}}_{PTC}$ is associated to a simulated $\mathbf{t}(\hat{\mathbf{g}}_{PTC})$, which is in general different from the measured TMI brightness temperature $\mathbf{t}_m$ from which $\hat{\mathbf{g}}_{PTC}$ is inferred. The difference is due to the additional information derived from PR measurements in the common swath. Consequently, this set of profiles when coupled with the observed TMI TBs constitutes a new specific cloud radiation database that could help in improving the estimation quality. This database may be referred to as "hybrid" since cloud simulations are associated to spaceborne measurements.

[37] Replacing $\mathbf{t}(\hat{\mathbf{g}}_{PTC})$ within the cloud radiation database with the corresponding TMI measurements $\mathbf{t}_m$, a calibration strategy can be envisaged. This means that we might think of simulated TBs as to be noisy and to "correct" them, i.e.,

$$\mathbf{t}_m(\hat{\mathbf{g}}_{PTC}) = \mathbf{t}(\hat{\mathbf{g}}_{PTC}) + \Delta\mathbf{t}(\hat{\mathbf{g}}_{PTC}) \tag{15}$$

The quantity $\Delta\mathbf{t}(\hat{\mathbf{g}}_{PTC})$ can be interpreted as a discrepancy (or perturbation) resulting from the contribution given by $\hat{\mathbf{g}}_{A,conv}$.

3.2.2.2. Outside the PR/TMI Common Swath

[38] When applying outside the common swath the BAMPR-P algorithm trained by the hybrid cloud radiation database, according to the Bayes theorem and similarly to equation (6), the a posteriori pdf can be written as:

$$p(\mathbf{g}|\mathbf{t}_m) = \frac{p[\boldsymbol{\varepsilon}_{\mathbf{t},cal}(\mathbf{g})]p(\mathbf{g})}{p(\mathbf{t}_m)} \tag{16}$$

being $\varepsilon_{t,cal}$ the "calibrated" total error:

$$\boldsymbol{\varepsilon}_{\mathbf{t},cal} = \mathbf{t}_m - \mathbf{t}_m(\hat{\mathbf{g}}_{PTC}) = \mathbf{t}_m - \mathbf{t}(\hat{\mathbf{g}}_{PTC}) + \Delta\mathbf{t}(\hat{\mathbf{g}}_{PTC}) \tag{17}$$

Each pdf in equation (16) is now specific to the atmospheric scenarios ingested into the hybrid cloud radiation database. In particular, $\boldsymbol{\varepsilon}_{\mathbf{t},cal}$ represents a more appropriate estimation of the error model that replace the one derived from the original cloud radiation database.

[39] Finally, the swath broadening profiles $\hat{\mathbf{g}}_B$, estimated by BAMPR-B, are given by:

$$\hat{\mathbf{g}}_B = \int_0^\infty \mathbf{g} \frac{p[\boldsymbol{\varepsilon}_{\mathbf{t},cal}(\mathbf{g})]p(\mathbf{g})}{p(\mathbf{t}_m)} d\mathbf{g} \tag{18}$$

From a practical point of view, the previous form of estimation for the swath broadening is applied only when at least one pixel "close enough" to $\mathbf{t}_m$ exists in the narrow swath. A TB is considered "close enough" if it falls within a sub-domain in the TB hyper-space centered on $\mathbf{t}_m$. The semi-axis of the sub-domain, approximated as an hyper-ellipsoid, is set equal to the standard deviation of $\boldsymbol{\varepsilon}_{\mathbf{t},cal}$. On the contrary, when the previous condition is not verified, the BAMPR-P retrieval is performed since the hybrid cloud radiation database can not be considered representative of the pixel under observation. It is important to point out that the PR swath synthetic broadening relies on the assumption of a substantial TB pattern homogeneity across the TMI swath.

[40] It is worth mentioning that BAMPR-B can be generalized, although only the implementation for a

single event has been discussed here. Hybrid cloud radiation databases specialized for various rainfall space-time typologies could be built based on the observation of precipitating systems relative to different geographical and seasonal conditions.

4. Tests on Synthetic Data

[41] In this section the combined inversion schemes, introduced in the previous section, are applied to simulated TMI and PR observations, generated as described in section 2. These tests aim at numerically proving that the proposed combination approach is able to improve the TMI-only retrieval.

4.1. Results Inside the Common TMI-PR Swath

[42] A simulated test has been carried out in order to evaluate the retrieval capability of the proposed BAMPR-C technique within the MMS framework. The training cloud radiation database consists of the minute 2130 of UW-NMS hurricane Bonnie simulation. A set of 600 profiles has been extracted to be used as synthetic test measurements. In order to have a statistically significant set, samples have been chosen according to their vertically integrated equivalent LWCs at PR resolution. A threshold of 5 kg/m^2 has been used for clustering the total ice water contents into low and high content classes. Similarly, for total hydrometeors in water phase two other thresholds at 5 kg/m^2 and 15 kg/m^2 have been set up to separate profiles having moderate, intermediate and high total LWCs. Six classes have been consequently obtained and 100 profiles have been randomly extracted from each of them, defining the synthetic measurements test set.

[43] The first two numerical tests have been carried out by using BAMPR-P and BAMPR-A. These two algorithms represent a reference to understand if the application of any combination technique brings some improvements to the estimation. For simplicity, synthetic TBs are calculated at nadir and with PR resolution as for reflectivities. We have also performed a retrieval using the TVM algorithm in order to understand how the cascade retrieval procedure, implemented within BAMPR-C, compares to it. For all the four methods, the results of the synthetic retrieval in terms of estimation errors have been summarized in Figure 5 and Table 1.

[44] Figure 5 shows the mean of estimated and a priori rain and graupel profiles. The difference between the two represents the error bias profile. Standard deviations of estimation error at each level are shown as well.

[45] When comparing the results of the BAMPR-A retrieval with the ones of BAMPR-P, while on one hand there is a noticeable improvement in the rain profile estimate brought by the active instrument, on the other hand it is apparent that graupel estimation performs poorly. This behavior is basically due to the reduced sensitivity of the PR reflectivities to the ice-phase particle contents. Using the TVM algorithm, the ice estimation is improved with respect to the use of reflectivities only (i.e., BAMPR-A), while the rain retrieval keeps similar performances. The BAMPR-C scores are similar to those of TVM scheme, being the overall performances only slightly degraded. The latter results suggest that the use of BAMPR-C, implemented for the TMI-PR combination inside the common swath, is a good compromise in terms of profile retrieval accuracy. Analogous conclusions can be derived when considering slanted TB observations [*Mugnai et al*., 2001].

[46] In Table 1 performances of the four retrieval algorithms in terms of rain columnar content, graupel columnar content and surface rain rate are summarized by means of error mean (bias), error standard deviation and correlation coefficients between estimated and "true" values. From this analysis it emerges that, especially for the retrieval of columnar contents, although TVM performances are the best, the ones of BAMPR-C are very close.

4.2. Results of the PR Swath Synthetic Broadening

[47] An internal test on synthetic data has been also performed to demonstrate the applicability of the swath broadening technique, as described in section 3.2.2. Profiles from the minute 2130 of the Bonnie hurricane simulation have been again used as a training database, while those from minute 2340 of the same simulation have been considered as synthetic test measurements.

[48] A portion of this domain having an extension of 300 km x 150 km (corresponding to 8820 profiles) has been considered as TMI-PR common swath. As a first step, PTC retrieval has been performed on this domain according to equation (14). Then, the PTC-retrieved profiles $\hat{\mathbf{g}}_{PTC}$, coupled with the synthetic measured TBs within the test domain, have been used as hybrid cloud radiation database. From the minute 2340 model output of the same simulation, a second portion with an extension of 25 km $\times$ 70 km (corresponding to 250 profiles) has been extracted as independent set of synthetic measurements. The statistics of the retrieval errors, obtained for these pixels by using BAMPR-P (original database) as well as BAMPR-B (hybrid database) algorithms, are compared in Table 2.

[49] It is apparent the improvement that, by exploiting the hybrid database information, BAMPR-B brings with respect to BAMPR-P in terms of estimation accuracy, especially for rainfall products.

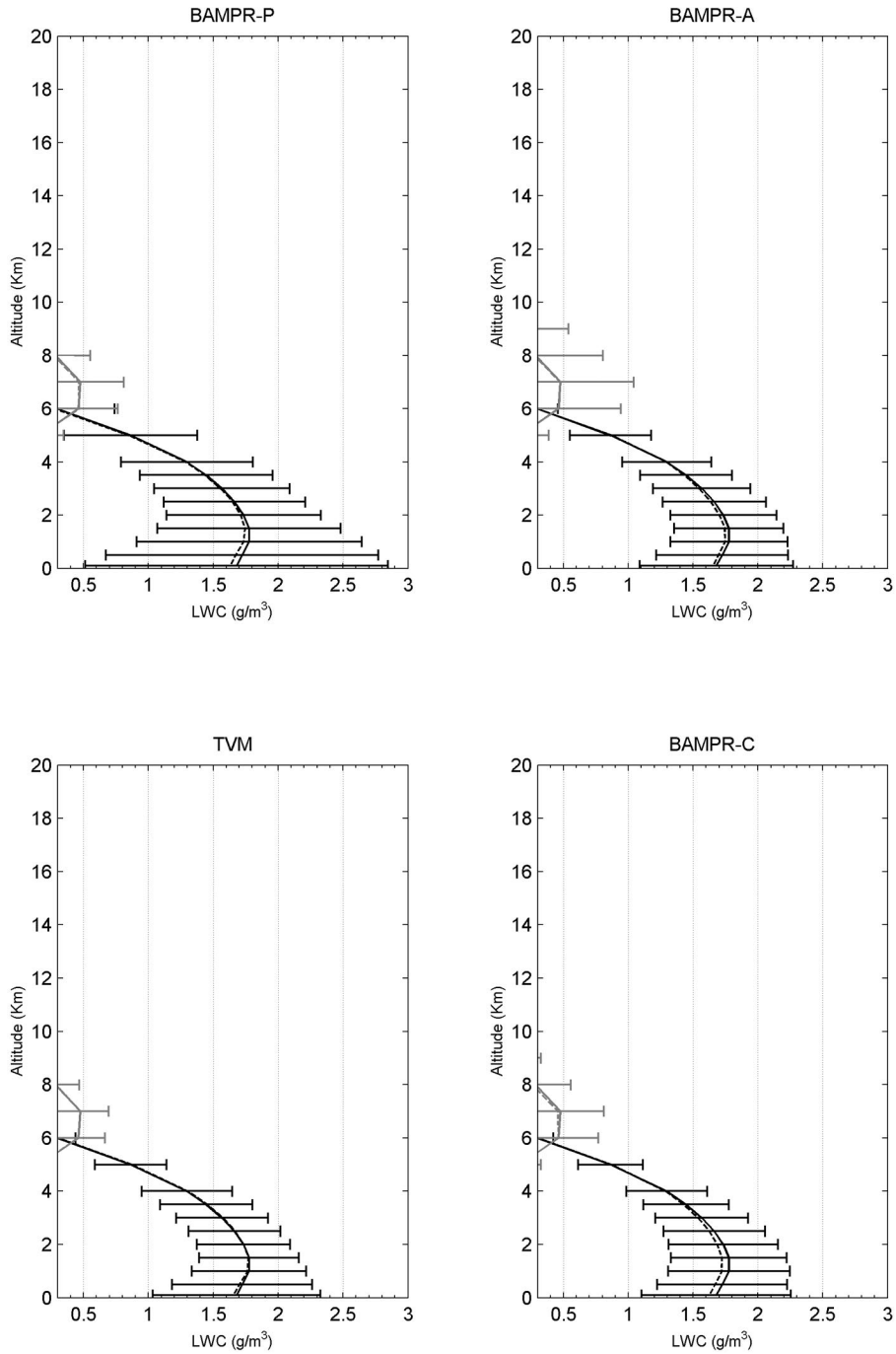

Figure 5. Results of the internal numerical tests, using (top left) BAMPR-P, (top right) BAMPR-A, (bottom left) TVM, and (bottom right) BAMPR-C for nadir-looking synthetic observations. Dashed lines indicate the a priori mean profile, solid lines indicate the estimated mean profile, and error bars represent error standard deviation at each level. Vertical profiles are such that solid lines are for rain, and shaded lines are for graupel equivalent LWC.

Table 1. Statistical Results of Internal Numerical Tests Using BAMPR-P, BAMPR-A, TVM, and BAMPR-C Retrieval Methods in Terms of Error Bias, Standard Deviation, and Correlation Coefficient for Columnar Rain Contents, Columnar Ice Contents, and Surface Rain Rate, Derived From Bonnie Hurricane Simulation

	Rain, kg/m^2			Graupel, kg/m^2			Surface Rain Rate, mm/h		
	Bias (8.41)[a]	SD	Correlation Coefficient	Bias (1.63)[a]	SD	Correlation Coefficient	Bias (38.2)[a]	SD	Correlation Coefficient
BAMPR-P	−0.14	2.01	0.97	−0.03	0.97	0.93	−1.1	25.8	0.76
BAMPR-A	−0.09	1.54	0.98	−0.04	2.46	0.50	−0.6	12.9	0.94
TVM	0.01	1.31	0.99	0.01	0.72	0.96	−0.6	14.1	0.93
BAMPR-C	−0.16	1.47	0.98	−0.09	1.25	0.88	−1.2	12.6	0.95

[a]For each quantity the mean value in the data set is given in parentheses.

5. Application to TRMM Data

[50] As an example of the combined BAMPR technique, we will focus on the data granule n. 4267 of 25 August 1998, when TRMM passed over the hurricane Bonnie in the most intense period of the cyclone evolution. This case has been selected for testing and comparing the various BAMPR algorithms because of the availability of the corresponding numerical simulation. By so doing, the mismatch between the real and simulated measurements is minimized [see *Tassa et al*., 2003], and therefore the different behavior of the results corresponding to the various versions of the BAMPR algorithm may be basically attributed to the different characteristics of the implemented techniques.

[51] Figure 6 shows the TMI images at 10, 37, and 85 GHz at vertical polarization and the map of the maximum measured PR reflectivity. In the portion of the swath common to both TMI and PR, the observed scene consists of a rainband with strong embedded updrafts, revealed by high reflectivities and very low TBs at 85 GHz.

5.1. Inside the Common TMI-PR Swath

[52] The BAMPR-C algorithm, as described in subsection 3.2.1, has been applied to the measurements along the nadir section of the aforementioned case-study. The PR reflectivities corrected for path attenuation and the TMI TBs represented in the two upper panels of Figure 7 show that this vertical cut is mainly stratiform with a strong convection core around the distance at 600 km.

[53] First, BAMPR-P is applied to TMI TBs to provide an estimation of the ice water content using equation (5). The obtained estimates are then matched with the PR reflectivity profiles and used within the TPC step of BAMPR-C to select the retrieval profiles according to equation (12). In Figure 7 the estimated LWC for graupel (at 6-km height) is plotted, as obtained from BAMPR-P and BAMPR-C. The smoother characteristic of the BAMPR-P estimates with respect to the TPC is due to the coarser resolution of its products (i.e., the TMI 37 GHz channel resolution), much lower than the PR one. To emphasize the importance of the first step, we have also performed a BAMPR-A retrieval using only PR data, thus disregarding the ice content retrieved from TMI. As expected, as shown again in Figure 7, the retrieved graupel LWC shows a fairly unrealistic behavior when TMI constraint is avoided. Finally, in Figure 7 the surface rain rate as retrieved from BAMPR-C is compared to the same quantity derived from the TRMM official algorithm for rainfall estimation from PR (2A25) [*Iguchi et al*., 2000]. It is noticeable the agreement over the whole section, except for the peak around km 600, corresponding to a strong convective core. In this portion, BAMPR-C reaches a maximum of 50 mm/h, while 2A25 overpasses 160 mm/h (not shown). This high value is maybe due to an exaggerated correction for the strong path-attenuation affecting PR measurements in heavy precipitating structures [*Nakamura and Ikai*, 2002].

Table 2. Statistical Results of Internal Numerical Tests Using BAMPR-P Retrieval Algorithm, Trained by the Standard Database, and BAMPR-B, Trained by the Hybrid Database Calibrated by Means of TMI Synthetic Measurements

	Rain			Graupel			Surface Rain Rate		
	Bias (11.9)[a]	SD	Correlation Coefficient	Bias (6.27)[a]	SD	Correlation Coefficient	Bias (26.9)[a]	SD	Correlation Coefficient
BAMPR-P using model database	−1.20	7.13	0.66	0.60	2.47	0.96	−0.5	22.3	0.55
BAMPR-B using hybrid database	−1.10	5.95	0.74	0.45	1.90	0.97	−0.6	18.1	0.68

[a]Error parameters are given as in Table 1, with the mean value of each quantity of the data set given in parentheses.

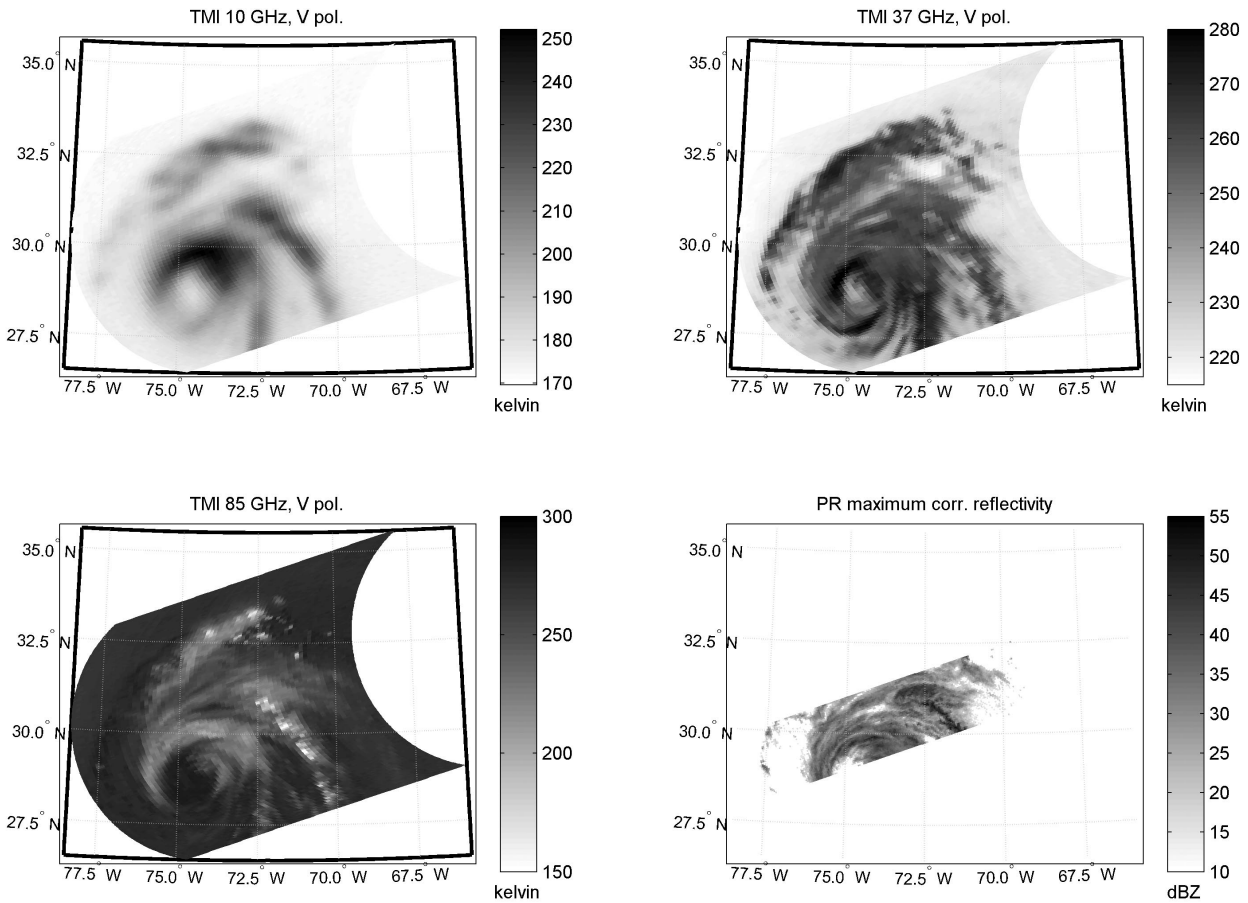

Figure 6. Hurricane Bonnie as remotely sensed by TRMM on 25 August 1998 (granule 4267). Clockwise from top left panel: maps of TMI brightness temperature at 10 GHz, 37 GHz, 85 GHz (vertical polarization), and maximum PR reflectivity corrected for path attenuation. See color version of this figure at the back of this issue.

5.2. Radar Swath Synthetic Broadening

[54] The case study of the previous sub-section is also used to show an application of the proposed swath broadening BAMPR-B technique. In the top panel of Figure 8 the TMI swath is overlapped with the PR one. In Figure 8, solid dots represent the TMI pixels of the common portion, used to perform the PTC retrieval in order to extract the TMI-calibrated cloud radiation database. The resulting hybrid database is used to perform BAMPR-B along a TMI scan line lying in the remaining portion of the PR swath, also indicated with solid dots in Figure 8. TMI TBs relative to this section are plotted in the middle panel of Figure 8. This independent cut has been chosen to test the behavior of the BAMPR-B comparing its retrieved surface rainfall rates with the ones derived from BAMPR-P and with the TRMM 2A25 estimates. These two products represent a reference for BAMPR-B, since the first one is a pure radiometric algorithm (no calibration), while the second is the official PR rainfall product. Resulting rain rate estimates as obtained from all the three methods are shown in the bottom panel of Figure 8. BAMPR-B shows a general tendency to drive BAMPR-P estimates toward the ones of TRMM-2A25, mitigating their discrepancies. This result confirms that the use of the hybrid cloud radiation database can help in providing a more accurate estimate outside the common swath.

6. Conclusions

[55] In this paper, we have proposed two combined retrieval techniques, called BAMPR-C and BAMPR-B, able to exploit the synergy of spaceborne radar and microwave radiometer having different scanning geom-

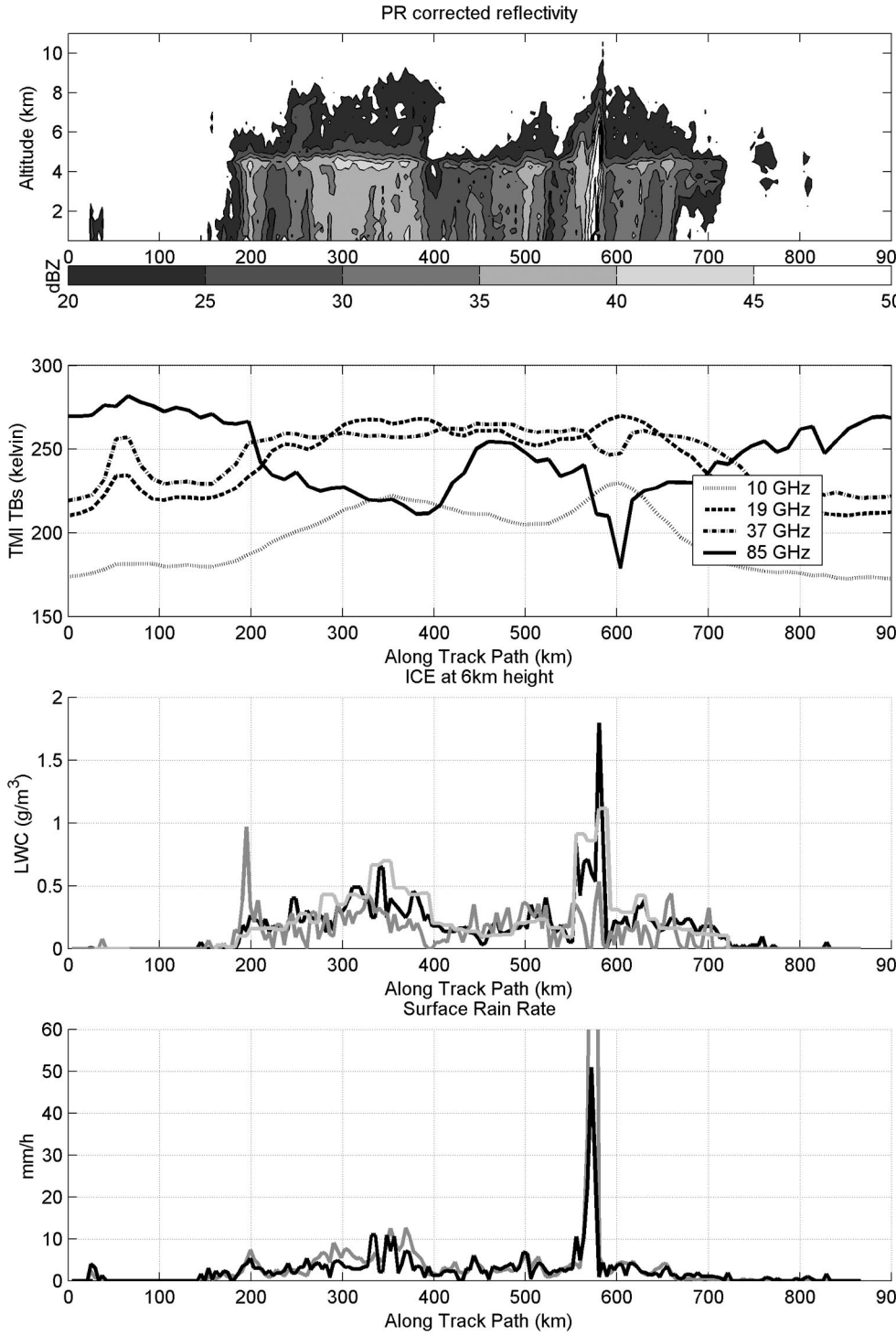

Figure 7. Nadir looking vertical cross section of PR corrected reflectivity (first panel) and vertically polarized brightness temperatures of TMI scan central pixel (second panel) for the case study of Figure 5. The third panel contains the corresponding retrieved graupel LWC at 6-km height by BAMPR-P (light shaded line), BAMPR-A (dark shaded line) and BAMPR-C (solid line), while the bottom panel shows the retrieved surface rain rate by BAMPR-C (solid line) and 2A25 TRMM official product (shaded line).

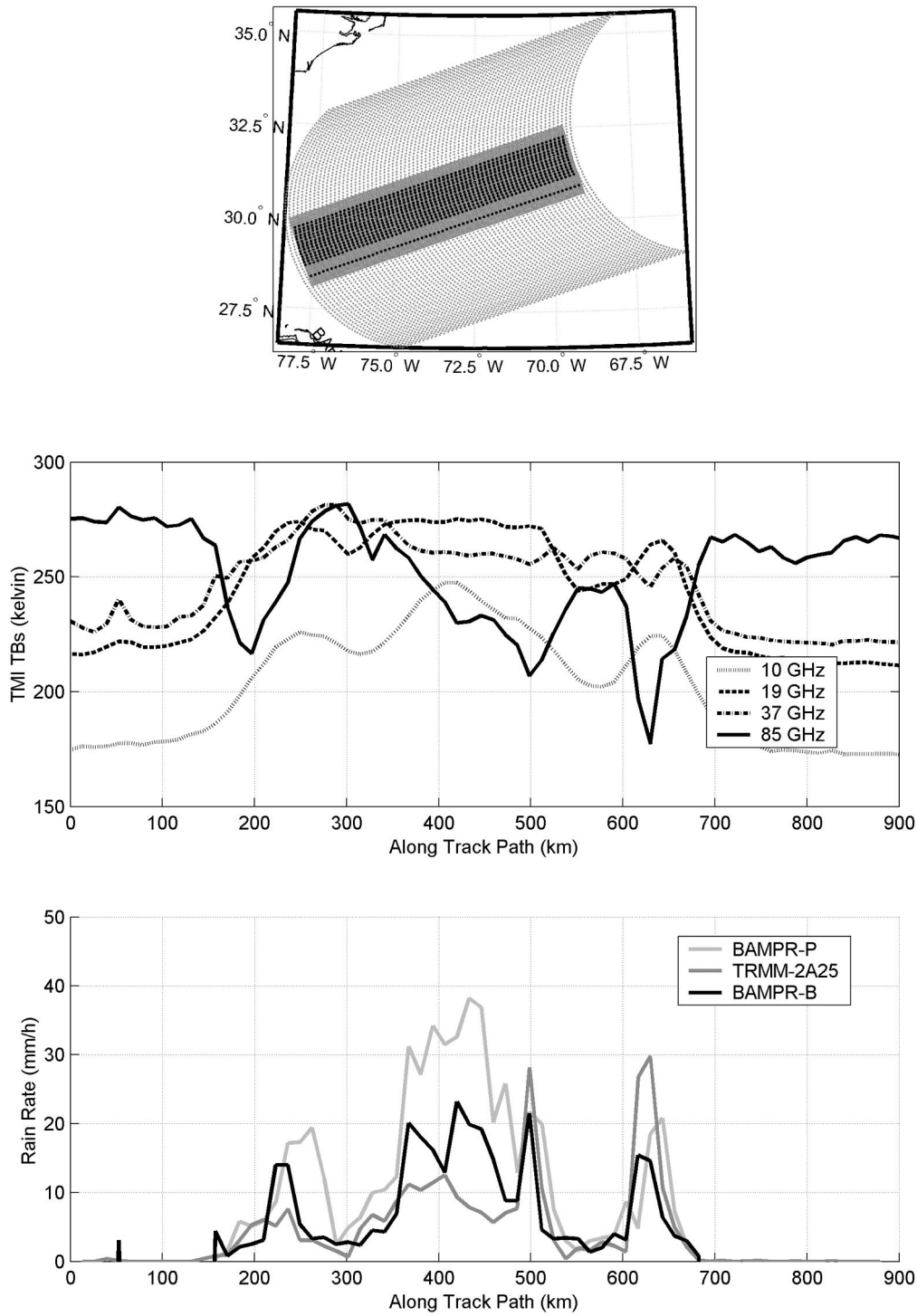

Figure 8. (top) PR and TMI swaths (shaded dots). The portion of PR swath in solid dots refers to the domain used to perform PTC retrieval, while the isolated scan line in solid dots represent the section selected for the application of swath broadening. (middle) TMI brightness temperatures (vertical polarization) corresponding to the along track section selected as independent set. (bottom) Surface rain rate estimates, obtained from BAMPR-P (light shaded curve), BAMPR-B (solid curve) and 2A25 TRMM official product (dark shaded curve).

etries. Their formulation in the framework of the Bayesian inversion theory has been illustrated by distinguishing the inversion inside (for BAMPR-C) and outside (for BAMPR-B) the common swath. Results obtained from numerical tests on synthetic measurements have demonstrated the capability of the two combined algorithms in improving single-sensor based estimates that make use of TMI or PR data only.

[56] The different techniques for implementing the BAMPR algorithm have been also applied to TRMM measurements for the case of hurricane Bonnie on 25 August 1998. It turns out that coupling TMI and PR information inside the common swath (BAMPR-C) provides ice profile estimates that appear more realistic than those obtained from PR data only. Moreover, the use of a radar swath synthetic broadening technique to generate a hybrid (cloud-model/PR) cloud radiation database (BAMPR-B) produces rainfall rate estimates outside the common swath that appear significantly better than those obtainable using the original cloud radiation database.

[57] This paper was actually intended to propose an inversion methodology more than describing an operational solution to the precipitation retrieval on a global scale. The potentials and limitations of the proposed combined algorithms are basically related to the proper generalization of the cloud radiation model, used as an a priori information within the inversion algorithm. Future works will be devoted to a throughout validation of the proposed methodology by using a larger set of TRMM data, possibly in combination with the ones of airborne field campaigns and ground–based sensors.

[58] **Acknowledgments.** This work has been supported by the European Commission through the EuroTRMM project (1997-2000), by the Italian National Group for Prevention from Hydrological Hazards (GNDCI), by the Italian Space Agency (ASI) and by the European Space Agency (ESA). We want to thank Prof. Gregory Tripoli and Dr. Giulia Panegrossi of the University of Wisconsin for providing the hurricane Bonnie simulation and for profitable interactions.

References

Bauer, P., L. Schanz, and L. Roberti, Correction of the three-dimensional effects for passive microwave remote sensing of convective clouds, *J. Appl. Meteorol.*, *37*, 1619–1632, 1998.

Grecu, M., and E. N. Anagnostou, Use of passive microwave observations in a radar rainfall-profiling algorithm, *J. Appl. Meteorol.*, *41*, 702–715, 2002.

Haddad, Z. S., S. L. Durden, and E. Im, Stochastic filtering of rain profiles using radar, surface-referenced radar, or combined radar-radiometer measurements, *J. Appl. Meteorol.*, *35*, 229–242, 1996.

Haddad, Z. S., E. A. Smith, C. D. Kummerow, T. Iguchi, M. R. Farrar, S. L. Durden, M. Alves, and W. S. Olson, The TRMM Day-1 radar/radiometer combined rain-profiling algorithm, *J. Meteorol. Soc. Jpn.*, *75*, 799–809, 1997.

Iguchi, T., T. Kozu, R. Meneghini, J. Awaka, and K. Okamoto, Rain-profiling algorithm for the TRMM precipitation radar, *J. Appl. Meteorol.*, *39*, 2038–2052, 2000.

Kummerow, C. D., W. S. Olson, and L. Giglio, A simplified scheme for obtaining precipitation and vertical hydrometeor profiles from passive microwave sensors, *IEEE Trans. Geosci. Remote Sens.*, *34*, 1223–1232, 1996.

Kummerow, C. D., W. Barnes, T. Kozu, J. Shiue, and J. Simpson, The Tropical Rainfall Measuring Mission (TRMM) sensor package, *J. Atmos. Oceanic Technol.*, *15*, 809–817, 1998.

Marzano, F. S., and P. Bauer, Sensitivity analysis of airborne microwave retrieval of stratiform precipitation to the melting layer parameterization, *IEEE Trans. Geosci. Remote Sens.*, *39*, 5–23, 2001.

Marzano, F. S., A. Mugnai, G. Panegrossi, N. Pierdicca, E. A. Smith, and J. Turk, Bayesian estimation of precipitating cloud parameters from combined measurements of spaceborne microwave radiometer and radar, *IEEE Trans. Geosci. Remote Sens.*, *37*, 596–613, 1999.

Marzano, F. S., S. Di Michele, A. Mugnai, and A. Tassa, Bayesian techniques for precipitation profile retrieval from spaceborne microwave radiometric sensors, paper presented at the 5th Pacific Remote Sensing Conference (PORSEC), Natl. Inst. of Oceanogr., Goa, India, 5–8 Dec. 2000.

Meneghini, R., T. Iguchi, T. Kozu, L. Liao, K. Okamoto, J. A. Jones, and J. Kwiatkowsky, Use of surface reference technique for path attenuation estimates from the TRMM Precipitation Radar, *J. Appl. Meteorol.*, *39*, 2053–2070, 2000.

Mugnai, A., E. A. Smith, and G. J. Tripoli, Foundations for statistical-physical precipitation retrieval from passive microwave satellite measurements. part II: Emission source and generalized weighting function properties of a time-dependent cloud-radiation model, *J. Appl. Meteorol.*, *32*, 17–39, 1993.

Mugnai, A., S. Di Michele, F. S. Marzano, and A. Tassa, Cloud-model based Bayesian techniques for precipitation profile retrieval from TRMM microwave sensors, in *Proceedings EuroTRMM Workshop on Assimilation of Clouds and Precipitation in NWP Models, Reading, (UK), Nov. 4–5, 2000,* pp. 323–345, Eur. Cent. for Medium-Range Weather Forecasts, Reading, UK, 2001.

Mugnai, A., A. Tassa, S. Di Michele, C. Adamo, S. Dietrich, S. Pinori, F. S. Marzano, G. Panegrossi, G. J. Tripoli, E. A. Smith, and J. P. V. Baptista, Potential improvements of rainfall estimation from the Global Precipitation Mission, in *Proceedings of the 2nd EGS Plinius Conference on Mediterranean Storms- Siena, Italy -October 2000, GNDCI Publ. N.2547*, edited by A. Mugnai, F. Guzzetti,

and G. Roth, pp. 91-108, Gruppo Naz. per la Difesa dalle Catastrofi Idrogeol., Perugia, Italy, 2002.

Nakamura, K., and J. Ikai, Comparison rain rates over ocean derived from TRMM Microwave Imager and Precipitation Radar, in *TRMM International Science Conference Abstracts (Honolulu, Hawaii, 22-26 July 2002)*, *NASA Tech. Memo., 2002-211605*, 2002.

Olson, W. S., C. D. Kummerow, G. M. Heymsfield, and L. Giglio, A method for combined passive-active microwave retrievals of cloud and precipitation parameters, *J. Appl. Meteorol.*, *35*, 1763–1789, 1996.

Panegrossi, G., S. Dietrich, F. S. Marzano, A. Mugnai, E. A. Smith, X. Xiang, G. J. Tripoli, P. K. Wang, and J. P. V. Poiares Baptista, Use of cloud model microphysics for passive microwave-based precipitation retrieval: Significance of consistency between model and measurement manifolds, *J. Atmos. Sci.*, *55*, 1644–1673, 1998.

Panegrossi, G., A. Tassa, S. Di Michele, G. J. Tripoli, A. Mugnai, and E. A. Smith, Using TRMM observations to improve numerical simulations of precipitation within tropical cyclones, paper presented at 81st AMS Annual Meeting, Symposium on Precipitation Extremes: Prediction, Impacts, and Responses, Am. Meteorol. Soc., Albuquerque, N. M., 14–18 Jan. 2001.

Pierdicca, N., F. S. Marzano, G. D'Auria, P. Basili, P. Ciotti, and A. Mugnai, Precipitation retrieval from spaceborne microwave radiometers using maximum a posteriori probability estimation, *IEEE Trans. Geosci. Remote Sens.*, *34*, 831–845, 1996.

Roberti, L., J. Haferman, and C. Kummerow, Microwave radiative transfer through horizontally inhomogeneous precipitating clouds, *J. Geophys. Res.*, *99*, 16,707–16,718, 1994.

Smith, E. A., F. J. Turk, M. R. Farrar, and X. Xiang, Estimating 13.8 GHz path-integrated attenuation from 10.7 GHz brightness temperatures for the TRMM PR-TMI precipitation algorithm, *J. Appl. Meteorol.*, *36*, 365–388, 1997.

Tassa, A., S. Di Michele, A. Mugnai, F. S. Marzano, and J. P. V. Poiares Baptista, Cloud-model based Bayesian technique for precipitation profile retrieval from TRMM microwave imager, *Radio Sci.*, *38*, doi:10.1029/2002RS002674, in press, 2003.

Tripoli, G. J., An explicit three-dimensional non-hydrostatic numerical simulation of a tropical cyclone, *Meteorol. Atmos. Phys.*, *49*, 229–254, 1992.

S. Di Michele, A. Mugnai, and A. Tassa, Istituto di Scienze dell'Atmosfera e del Clima (ISAC), Consiglio Nazionale delle Ricerche (CNR), Via del Fosso del Cavaliere 100, 00133 Roma, Italy. (s.dimichele@isac.cnr.it)

F. S. Marzano, Dipartimento di Ingegneria Elettrica, Centro di Eccellenza CETEMPS, Università dell'Aquila, Monteluco di Roio, 67040 L'Aquila, Italy.

J. P. V. Poiares Baptista, ESTEC, European Space Agency, 2200 AG, Noordwijk, Netherlands.

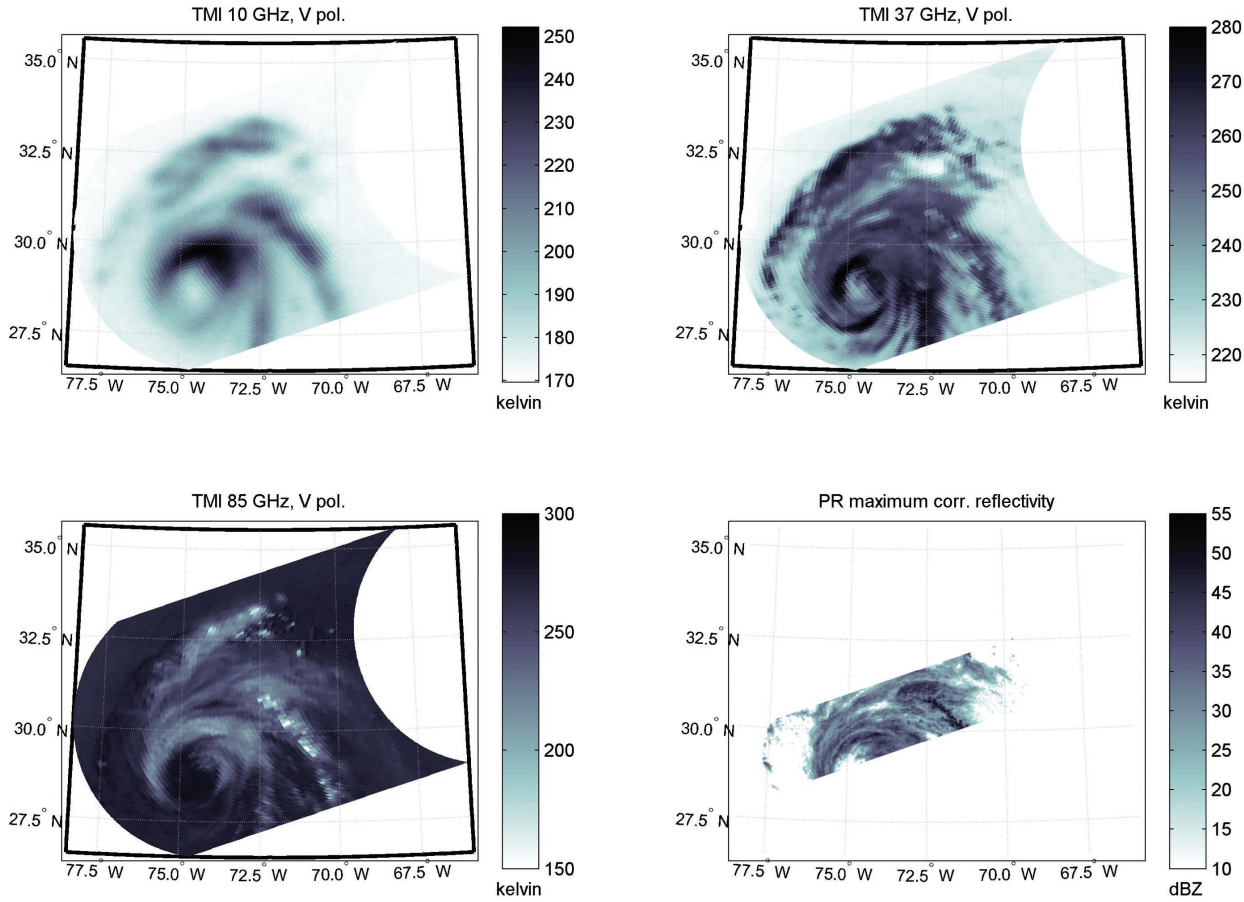

Figure 6. Hurricane Bonnie as remotely sensed by TRMM on 25 August 1998 (granule 4267). Clockwise from top left panel: maps of TMI brightness temperature at 10 GHz, 37 GHz, 85 GHz (vertical polarization), and maximum PR reflectivity corrected for path attenuation.